Arsenic and phosphorus association with iron nanoparticles between streams and aquifers: implications for arsenic mobility

Adam Hartland[*a], *Joshua R. Larsen*[b], *Martin S. Andersen*[c], *Mohammed Baalousha*[d], *Denis O'Carroll*[c]

[a]Environmental Research Institute, School of Science, Faculty of Science and Engineering, University of Waikato, Hamilton, New Zealand

[b]School of Geography, Planning and Environmental Management, The University of Queensland, Australia

[c]Connected Waters Initiative Research Centre, UNSW Australia, 110 King Street, Manly Vale, NSW 2093, Australia

[d]Centre for Environmental NanoScience and Risk, Arnold School of Public Health, University of South Carolina, Columbia, USA

ABSTRACT

The microbial oxidation of organic matter coupled to reductive iron oxide dissolution is widely recognized as the dominant mechanism driving elevated arsenic (As) concentrations in aquifers. This paper considers the potential of nanoparticles to increase the mobility of As in aquifers thereby accounting for discrepancies between predicted and observed As transport reported elsewhere. Arsenic, phosphorus and iron size distributions and natural organic matter association were examined along a flow path from surface water via the hyporheic zone to shallow groundwater. Our analysis demonstrates that colloidal Fe concentration (> 1 kDa) correlates with both colloidal P and colloidal As concentrations. Importantly, increases in the concentration of colloidal P (> 1 kDa) were positively correlated with increases in nominally dissolved As (< 1 kDa), but no correlation was observed between colloidal As and nominally dissolved P. This suggests that P actively competes for adsorption sites on Fe nanoparticles, displacing adsorbed As, thus mirroring their interaction with Fe oxides in the aquifer matrix. Dynamic redox fronts at the interface between streams and aquifers may therefore provide globally widespread conditions for the generation of Fe nanoparticles, a mobile phase for As adsorption currently unaccounted for in reactive transport models.

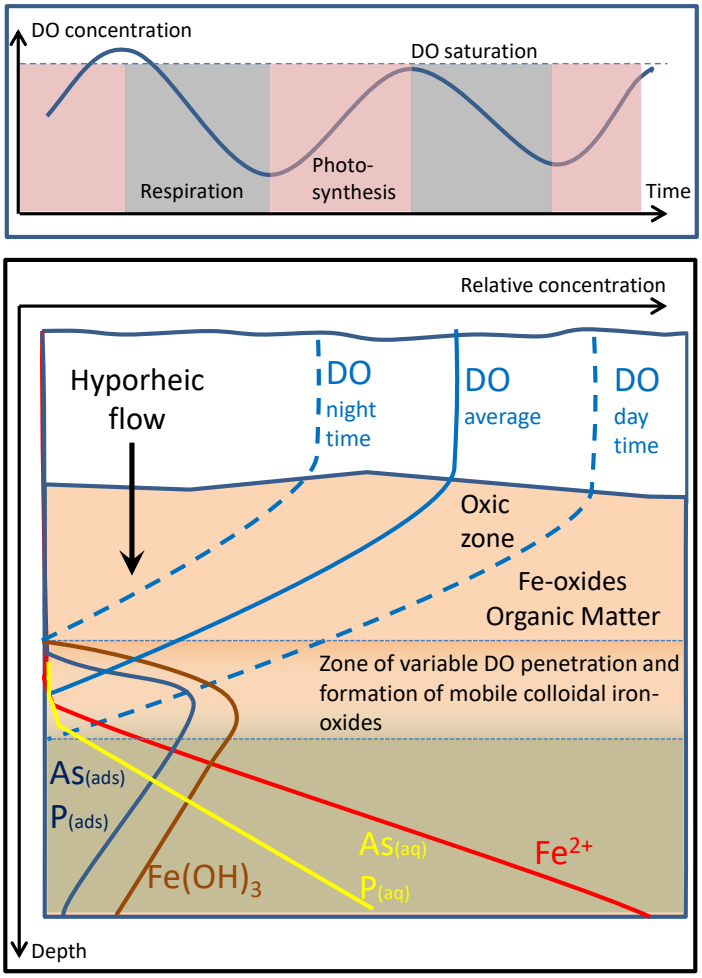

Scheme 1. Conceptual model of geochemical conditions driving Fe nanoparticle generation and surface adsorption of As and P.

INTRODUCTION

High levels of dissolved arsenic (As) in aquifers pose risks to human health when aquifers are used as the primary water resource[1-3]. Sub-oxic conditions prevail within many aquifers due to the microbial oxidation of organic matter of either sedimentary origin, or dissolved organic matter (DOM) predominantly derived from infiltration[4]. Both of these pathways increase the mobility of As via Fe oxide reduction and dissolution[5-7], assuming dissolved oxygen (DO) and other electron acceptors such as NO_3^- have already been consumed[8, 9]. Once mobilized, the mobility of As is mainly controlled by re-adsorption to aquifer sediments and through re-precipitation of As in Fe(III)-oxides[10]. A general model of As mobility in sedimentary aquifers remains elusive[10], in part because the adsorption behaviour of As on natural sediments[11, 12] differs markedly from As adsorption on synthetic Fe-oxides, against which surface complexation models have been developed[13]. Nevertheless, the close similarity and linear nature of As(III) adsorption isotherms for different age aquifer sediments suggests that a narrow range of distribution coefficients should adequately describe the retardation of As(III) due to adsorption in aquifers[10]. The fact that estimates of As retardation based on field data[14], and a push-pull experiment[11], are between ~4 to ~10 times less than this theoretical value, means that additional reactive transport mechanisms are required.

A key question is therefore why As mobility within sediments is greater than current theory would predict. Aquifer heterogeneity, accessibility of adsorption sites, formation of thioarsenate species[15], and potential competition by orthophosphate are undoubtedly important factors[10]. However, a third process: the transport of As on colloid (solids with dimensions between 1 and 1000 nm) and nanoparticle (a subset of colloids between 1 and 100 nm) surfaces, also has the potential to enhance the mobility of As in aquifers, by

64 bypassing adsorption on immobile solids that are usually assumed to account exclusively for
65 As retardation.

66 The stability of abundant Fe-rich nanoparticles with dimensions between 1 and 100 nm in
67 sub-oxic groundwater has been demonstrated when minimally-perturbing sampling
68 protocols[16] and a range of characterization methods are used[16-18]. Furthermore, iron- and
69 carbon-bearing colloids have been shown to associate with As in a series of field-based
70 studies employing size-fractionation[18-22]. While these results reinforce data from column
71 experiments which highlight the potential for colloid-facilitated transport of As in aquifers[23,
72 24], these studies have not conclusively demonstrated the significance of colloidal phases for
73 As speciation in groundwater, or the significance of this for As mobility more generally.

74 Previous studies of colloidal As in aquifers have employed filter membranes with a variety of
75 molecular weight cut offs (MWCO) and have variously defined 'truly dissolved' fractions
76 based on 10 - 5 kDa membranes (and as high as 0.45 μm in some instances[19, 22]). This is
77 problematic since it implies that As in 10 – 5 kDa filter permeates exists as either free ions or
78 inorganic complexes[20, 22]. However, colloid characterization work to date from natural
79 aqueous environments, including shallow groundwaters, demonstrates that nanoparticles with
80 the smallest dimensions may not be retained by these membranes[16] and are the most
81 important in terms of reactivity (due to higher surface/volume ratios)[16, 17]. Therefore, there is
82 an important need to improve our understanding of potential nano-scale associated As that
83 does not conform to the current assumptions of purely dissolved phase behaviour.

84

85 The effect of competing ions on the distribution of As within the colloidal and
86 nanoparticulate size range has also not been previously examined[19, 22]. This is an important

87 oversight to address since the existing literature on As adsorption to sedimentary minerals
88 such as iron oxides with isoelectric points > 7 (i.e. possessing positive charge states at
89 circumneutral pH[25]), clearly identifies orthophosphate PO_4^{3-} (and its protonated forms) as the
90 dominant competitor for suitable surface sites[10]. It is therefore reasonable to assume that the
91 same holds for adsorption to iron-bearing nanoparticles and colloids.

92

93 The association of As with colloids and nanoparticles also implies that As mobility in
94 aquifers may not only be controlled by complexation with stationary sediment surfaces, but
95 could also be retained within the flow path taken by colloids. The flow path and transit time
96 of water from surface to aquifers (and vice versa) is therefore an important consideration.
97 Several studies have suggested that groundwater flowing through palaeo-channel deposits
98 containing sedimentary organic matter can lead to As release[26, 27]. Alternatively, sub-oxic
99 conditions may develop at the surface within ponded water environments[28-30] due to high
100 inputs of organic matter, and the reductive dissolution of Fe-oxides during infiltration to
101 underlying aquifers. Interestingly, river channel networks also provide an exchange pathway
102 between surface waters and aquifers[31, 32], but have received comparatively little attention for
103 transport of contaminants such as As.

104

105 This study provides new data on the interaction between iron-bearing nanoparticles, arsenic
106 and phosphorus between streams and aquifers, and addresses the lack of information from
107 modern channel networks by presenting elemental data from size-fractionated water samples
108 from a surface water, hyporheic zone, shallow groundwater transect. These data show that P

competes with As for adsorption to Fe nanoparticle surfaces, which provide a mobile phase for As transport not currently accounted for in As transport models.

MATERIALS AND METHODS

Study site

This study was conducted across a transect of Maules Creek, a tributary of the Namoi River, located on the western slopes of the Great Dividing Range, New South Wales (NSW), Australia (Figure S1). The creek and its catchment have been described in detail elsewhere[33]. The aquifer material comprises coarse alluvium (well-rounded cobbles) and sand derived from weathering of Tertiary basalts and other volcanic rocks, derived from the Nandewar Range. Arsenic concentrations ranging between 1 and 14 μg L^{-1} have been consistently recorded at the site, with the higher concentrations occurring almost exclusively in the shallow, reduced (oxygen-depleted) sediments immediately beneath the stream. We targeted a series of monitoring piezometers that encompass both regional groundwater adjacent to the creek, groundwater within the banks and margins of the creek, and hyporheic zone water which actively exchanges with the surface water, immediately adjacent to and beneath the stream.

Groundwater sampling

Groundwater from shallow piezometers was obtained using a small peristaltic pump at very low flow rates (~0.5 – 1 L min^{-1}). Water chemistry (DO, pH and electrical conductivity [EC]) was monitored using a flow-cell until parameters stabilized (Table S1). Samples were then

taken in pre-cleaned LDPE bottles, rinsed three times with fresh groundwater and then carefully filled without head space. The samples were then immediately transferred to a field laboratory.

Fractionation protocol

Water samples were immediately filtered on-site under purified nitrogen gas to prevent oxidation. Following removal of an aliquot of the total (unfiltered) sample, the unfiltered sample was transferred to an ultrafiltration system and filtered under 4 bar zero-grade N_2 (Spectrum Labs, USA) using regenerated cellulose membranes (EMD Millipore, USA) with pore sizes of 100 kDa, 10 kDa and 1 kDa. Each sample fraction was collected in a Nalgene HDPE bottle and acidified to 2% acidity with trace analysis grade HNO_3 (Sigma Aldrich).

The filter fractions from this study were classified on the basis of relative size, but because there is no direct relation between molecular ~~size~~ weight (daltons) and length (nanometers) these size fractions are relative and do not specifically correspond to particle diameters. Five fractions are defined here: Large nanoparticles and colloids (> 100 kDa; > ~50 nm), Small nanoparticles (100 – 10 kDa; ~50 nm - ~10 nm), Fine nanoparticles (10 – 1 kDa; ~1 nm – ~10 nm), Nominally dissolved (< 1 kDa; < ~1 nm), and Colloidal (> 1 kDa; > ~1 nm).

As an additional measure, an aliquot of the total sample was passed through an ISOLUTE ENV+ solid phase extraction column immediately following collection. The ENV+ column is a wettable, non-polar (strongly hydrophobic) phase, which effectively sorbs the non-polar constituents of natural organic compounds. This step was undertaken as a rapid means (operation complete in < 10 s) of semi-quantitatively isolating the trace species that were present in association with natural organic matter (NOM).

All ultrafiltration components which came into contact with the sample were acid-washed with 10% HNO_3 and deionized water (DIW) between samples. Filtration rates were monitored at regular intervals to ensure that rates were consistent through time and that blocking of membrane pores was not occurring to a significant extent, thereby affecting the membrane pore size and size-based exclusion of particles.

Particle characterization

Samples were prepared for analysis by atomic force microscopy (AFM) by direct centrifugation immediately upon return to the laboratory following storage in the dark at 5 °C in bottles with no head space. The sample was centrifuged in a sealed Falcon tube (Fischer Scientific) with zero headspace at 11,400 g using an Allegra centrifuge (Beckman Coulter) equipped with an FX6100 rotor for six hours, thereby forcing all particles out of solution and onto a freshly-cleaved mica sheet. The centrifugation method minimizes aggregation and salt crystallization frequently encountered in drop drying methods widely used in the literature[34, 35], and enables detection of low nanoparticle concentrations present in groundwater[36]. While all reasonable steps were taken to minimize the potential for oxidation of Fe(II) to Fe(III) oxides during AFM sample preparation, we acknowledge that some potential for oxidation of the samples existed and therefore the results are interpreted accordingly.

Atomic Force Microscopy

Atomic Force Microscopy (AFM) analyses were performed using an XE-100 AFM (Park systems Corp., Suwon, Korea). The measurements were carried out in true non-contact mode using a Silicon cantilever with a typical spring constant of 42 N m^{-1} (PPP-NCHR, Park systems Corp., Suwon, Korea). All scans were performed at ambient conditions, which have been shown to produce accurate sizing, despite loss of most, but not all water[35]. Images were

recorded in topography mode with a pixel size resolution of 256 × 256 and a scan rate of 0.5-1.0 Hz. Images were collected from 15-20 random areas on each substrate, and a minimum of 200 height measurements were performed using the transect analysis using the XEI data processing and analysis software of the microscope (Park Systems Corp., Suwon, Korea). This number of images and height measurements has been shown to be sufficient to produce a representative particle size distribution[34, 36]. The measured heights were then classified into intervals of 0.5 nm to construct particle size distribution histograms, which were fitted with a log-normal distribution function as described elsewhere[34].

Water sample analysis

Dissolved organic carbon (DOC) concentrations and stable isotope ratios were determined for all samples by TOC-CRDS using methods reported elsewhere[37]. Samples for trace elements were analysed by ICP-MS. Detection limits were typically better than 0.5 mg L^{-1} for major ions and 0.1 μg L^{-1} for trace elements. Analyses of deionized water and acid blanks were below detection limits. Internal (within-run) precision was better than ± 0.05 μg L^{-1} for all elements, and overall (external) precision is estimated at 0.1 μg L^{-1} for all elements.

Reproducibility

ICP-MS analysis of procedural replicates (four fractionated samples [EC3, EC4, E3 and E4]), was used to calculate pooled standard deviations for trace elements in the total, < 100 kDa, < 10 kDa, < 1 kDa and ENV+ fractions (Equation 1).

$$s_{pooled} = \sqrt{\frac{(n_1 - 1)s_1^2 + (n_2 - 1)s_2^2 + \ldots + (n_k - 1)s_k^2}{n_1 + n_2 + \ldots + n_k - k}} \quad (1)$$

where k is the number of samples, s_1, s_2, etc. are the standard deviations of the replicated analyses, n_1, n_2, etc. are the numbers of measurements made for different samples.

Values of s_{pooled} (n=2, k=4) for Fe, P, As and V in mg L^{-1} are given in Table S2. This analysis demonstrates that the overall procedural error associated with the fractionation and subsequent elemental analysis of colloidal fractions was generally very good (< 1% RSD), with Fe being slightly more variable (< 5% RSD), and the organic fraction defined procedurally using the ENV+ resins being the most variable (< 19% RSD). Cumulative values of s_{pooled} (based on the addition of (s_{pooled}^2) in each fraction) were used in the calculation of the error associated with the colloidal fractions analysed in this study.

RESULTS AND DISCUSSION

AFM particle characterization and size distributions

Representative AFM-derived size distribution histograms (intervals of 0.5 nm) with log-normal fits[35] and AFM images are shown in Figure 1, and average particle size data are given in Table 1. The AFM data demonstrate that particles in all samples were dominated by nanoparticles with dimensions between 1 and 20 nm. Particles with heights > 25 nm formed only a significant proportion of the sample from the regional ground water (MBH piezometer, Figure 2). Between the river and shallow hyporheic zone (0.5 m), particle sizes dropped significantly from 10.2±17.9 nm to 1.7±1.0 nm (raw data), suggesting larger colloidal particles were filtered by river bed sediments. Within the hyporheic zone (Table 1, Figure 1a-c), there is a trend toward increasing particle size with depth, consistent with the precipitation of nano-scale Fe oxides and their subsequent aggregation along the flow path and/or the

219 greater filtration efficiency of smaller nanoparticles consistent with colloid filtration theory
220 (i.e., due to the large Brownian motion associated with smaller nanoparticles)[38-40].

221 AFM images (Figure 1; Figure S2) also showed some structures consistent with fibrillar
222 organic substances, such as polysaccharides, which can increase the size of nanoparticles and
223 colloids through aggregation, and which are exudates from aquatic organisms such as
224 bacteria and algae, therefore indicative of biological activity[41]. Fibrillar structures were most
225 prevalent in the surface water column, followed by the shallow (0.5 m) hyporheic zone
226 (Figure S2). The river water also contained very small particles and some larger, globular
227 nanoparticles of several 10s of nanometers in height, typical of natural organic colloids[42].
228 Moving along the flow path from the river to the aquifer, the shallow hyporheic zone was
229 characterised by very small colloidal particles, e.g. dispersed humic-like NOM[41]. In the mid-
230 hyporheic zone, colloid aggregation was evident (Figure 1b). This can be due to sample
231 preparation and there is a risk this is not representative of aggregation under natural
232 conditions. However, given that all samples were treated equally, this is considered unlikely.
233 In the mid- and deep-hyporheic zone, a very high number of particles were attached to the
234 AFM (mica) sheets (Figure 1c). This is consistent with the high concentration of total
235 colloidal iron at this depth (Table S3; see next section). Overall, the particle size distributions
236 suggest relatively mono-disperse distributions of small nanoparticles dominate the hyporheic
237 zone (Figure 1). It is possible that these very small nanoparticles may have experienced
238 reduced aggregation through charge and/or steric stabilization by NOM coatings[41]. In the
239 oxic regional ground water (MBH bore), the formation of large aggregates of several 10s of
240 nm in height was observed. Particles in this domain consisted of two populations: (i) small
241 around 1-3 nm in height and (ii) large around 10-30 nm in height.

242

243 *Fe, As and P in fractionated water samples*

244 Ultrafiltration of fresh river and groundwater samples at MWCO nominal pore sizes of 100,
245 10 and 1 kDa as well as natural organic matter (NOM) retention on ENV+ resins was used to
246 quantify the proportions of iron, phosphorus and arsenic associated with colloidal material
247 and NOM in the water samples. These results are presented in detail in Table S3.

248 The oxic river water and oxic regional groundwater were characterized by low total
249 concentrations of Fe, P and As: Fe 1.80-2.40 μmol L^{-1} (regional groundwater), 3.20 μmol L^{-1}
250 (river); P 6.10-10.6 μmol L^{-1} (regional groundwater), 3.27 μmol L^{-1} (river); As 0.05-0.09
251 μmol L^{-1} (regional groundwater), 0.01 μmol L^{-1} (river). Whereas, the reduced groundwater
252 below the stream channel had elevated total concentrations of Fe, but only marginally higher
253 P and As: Fe 1.10-88.6 μmol L^{-1}; P 3.3 – 11.8 μmol L^{-1}; As 0.02 – 0.10 μmol L^{-1} (Table S3).
254 Generalizing across the whole dataset, the hyporheic zone had the highest concentrations of
255 Fe, As and P.

256 In the river, Fe was dominantly colloidal, ~95% of Fe and 100% of P was associated with
257 particles greater than 100 kDa. Around 50% of riverine Fe was retained by the ENV+
258 column, but no ENV+ retention of P or As was observed (Table S3). Although, ENV+ did
259 not retain As, filtration between 10 and 1 kDa removed all of the As in the river sample. In
260 the oxic regional groundwater Fe was dominantly colloidal, whereas As was mainly
261 dissolved. Specifically, ~48% of Fe was removed by filtration at 100 kDa, and 49% between
262 100 and 1 kDa. For As, ~36% was colloidal, and ~64% of was nominally dissolved (Figure
263 2; Table S3).

264 The sub-oxic hyporheic zone had higher total concentrations of Fe and As as well as elevated
265 proportions of colloidal Fe, P and As (Figure 2; Table S3). The shallow hyporheic zone (0.5

m) water was closer to river water in composition, with comparable total Fe and P (within 1 μmol L-1), ~40% higher total As, and negligible colloidal As (~93% of As nominally dissolved) and no significant ENV+ retention of As. DO had decreased from ~5 mg L^{-1} in the river to less than 1 mg L^{-1} in the hyporheic zone, consistent with its consumption through the oxidation of labile organic matter along the flow path as shown by the progressive enrichment of DOC-$\delta^{13}C$ values[37] by +1.4‰ between the 0.5 m and 1.5 m hyporheic piezometers (Table S4). In the mid-hyporheic zone (1 m) total As had increased by ~60% relative to the shallow hyporheic piezometer with ~48% of As and ~72% of Fe associated with nanoparticles between 100 and 1 kDa, and ~15% of total As retained by the ENV+ column. Finally, in the deep hyporheic piezometer (1.5 m), total As had increased by a factor of 2 relative to the shallow hyporheic piezometer, ~80% of Fe and ~20% of As was now associated with colloids, and ~80% of total As was nominally dissolved. Analysis of the ENV+ permeate indicated that no As was associated with hydrophobic organic constituents, but ~15% of P and ~98% of Fe were associated with NOM in the deepest hyporheic zone (1.5 m). Because the ENV+ column retains NOM by hydrophobic interactions, it is possible that a hydrophilic fraction of NOM, not captured by our fractionation protocol, played a role in the partitioning of As between colloidal and nominally dissolved (< 1 kDa) fractions.

Ultrafiltration of the hyporheic zone samples revealed an increasing degree of association between Fe and the small and fine nanoparticle fractions with increasing depth (< 10 kDa and <1 kDa, respectively) (Figure 2). Conversely, the AFM data (Table 1) show an increase in particle size with depth. This implies that the AFM data, which show size distribution of all types of colloids and nanoparticles, may reflect particle aggregation along the flow path. Whereas, the Fe ultrafiltration data are consistent with the formation of small Fe oxide nanoparticles at the interface of the oxic river water and reduced, shallow groundwater

beneath the hyporheic zone. Furthermore, the increase in Fe concentration in the deepest hyporheic piezometer (1.5 m) is indicative of secondary dissolution of Fe nanoparticles further along the flow path.

The interrelationship between the colloidal distributions of Fe, P and As and their variable association with NOM supports the interpretation that Fe oxide nanoparticles, potentially coated in NOM, were abundant in the shallow hyporheic zone. This inference is supported by the consistent relationship between colloidal Fe concentration and Fe retention by ENV+ (Figure S4). Based on these data, it appears that elevated colloidal Fe and As was linked to the presence of a redox front, driven by the supply of labile organic matter and DO from the infiltrating surface water. Overall, the colloidal As fraction in the water samples ranged from ~0 to ~48%, averaging 13% ± 15% (1σ) with the greatest concentration of colloidal As being detected in the mid-hyporheic zone. These results are therefore also comparable to previous studies that have utilized field ultrafiltration protocols[19, 22]. A study of As in the alluvial aquifers of West Bengal, India[19], found ~6 to ~17% of As was associated with colloids, based on a finest MWCO of 5 kDa. Using a finest MWCO of 10 kDa, researchers in Bangladesh[22] found the colloidal fraction of As to be between 0 and ~40% in groundwater, and up to ~50% in soil waters sampled beneath flooded paddy fields. In combination these data demonstrate a significant, if variable, association between As and colloidal phases in aquifers. This also supports the interpretation that Fe is dominantly colloidal, and probably present in a continuum between freshly precipitated meta-stable amorphous iron oxides, and Fe(II) ions held in complexes with NOM which are transported into sub-oxic environments.

Interactions between Fe, P and As

313 Data presented in Figure 3 indicate a range of interactions between Fe, P and As. For the
314 coarsest fraction (> 100 kDa), P association with coarse colloids appears to increase in a
315 fairly linear fashion with increases in Fe, yet As shows no association with the coarsest
316 fraction of Fe (Figure 3a-b). No saturation with respect to Fe and P bearing solids was
317 observed in a PHREEQC speciation analysis of these water samples, implying that the
318 relation between Fe and P (Figure 3a) corresponds to an adsorption process. For samples
319 filtered out between 100 and 10 kDa (Figure 3c-d), As and P concentrations show similar
320 linear relationships with Fe concentration in the same fraction. Finally, P and As data from
321 the finest fraction (10 – 1 kDa) show no correlation with Fe. Although total Fe concentrations
322 in these fractions ranged between 0 and 35 μmol L^{-1} (Figure 3e-f), it is likely that this Fe was
323 present as Fe(II) ions with some degree of complexation by NOM (Table S3).

324

325 *Evidence for competition between As and P for Fe nanoparticles*

326 In the context of the total surface loading of iron colloids by oxyanions (assuming this is the
327 dominant reaction mechanism controlling P, V and As), adsorption is clearly dominated by
328 orthophosphate, in the order P-PO_4^{3-} >> As-H_3AsO_3 >> V-VOH_3 (Table S3). At the ambient
329 pH of the system, 6.4 to 7.4 (Table S1), the PHREEQC speciation indicates that the relevant
330 species to consider in sorption reactions are $H_2PO_4^-$/HPO_4^{2-} and for arsenic H_3AsO_3/$H_2AsO_3^-$
331 /$HAsO_4^{2-}$. In Figure S5, the total apparent oxyanion adsorption (to colloidal surfaces) is
332 plotted as a function of the colloidal Fe concentration. There appears to be a linear
333 component (Figure S5), but there are additional second-order effects which may relate to a
334 change in nanoparticle morphology, e.g. aggregation or Ostwald ripening to more crystalline
335 forms of Fe oxides with different surface characteristics. Nevertheless, these data clearly
336 demonstrate the importance of Fe-bearing colloids for the behaviour of oxyanion species.

Although P clearly dominates in this system, there is an identifiable effect of increasing P surface loading on the size distribution of As, since the concentration in the nominally dissolved fraction (< 1 kDa) increases as the colloidal P concentration increases (Figure 4a; R^2= 0.59). This increase in nominally dissolved As is accompanied by a corresponding reduction in the nominally dissolved concentration of P (Figure 4a; Table S3), further supporting the argument that P adsorption to colloid surfaces occurs to some extent by displacement of As ions. This is consistent with previous studies[10] which show As(III) adsorption to Fe oxides in aquifer sediments to be completely reversible and the same would be expected for As(III) adsorption to Fe oxide nanoparticles. Furthermore, these data do not support the competitive displacement of P by As (Figure 4b), which again, is consistent with the literature on As/P adsorption behaviour[10]. Finally, we reanalyzed the data from the only other study of colloidal Fe, P and As interactions in groundwater[22] (Figure S6) and found very similar relationships between Fe, P and As. This therefore indicates that competition by P for colloidal Fe phases may be a widespread phenomenon with significant implications for As transport in aquifers.

Potential for colloid-facilitated transport of arsenic in sedimentary aquifers

In order to assess the potential for transport of As-bearing colloids, colloid filtration theory can be used to quantify expected nanoparticle, and associated arsenic, travel distances above a threshold normalized nanoparticle concentration (1% in this case)[43]:

$$L = \frac{-2d_C}{3(1-e)\,\eta_O\,\alpha}\ln\left(\frac{C}{C_O}\right) \qquad (2)$$

where C/C_o is the normalized nanoparticle concentration in the aqueous phase, e is porosity, α is the attachment efficiency (i.e., number of nanoparticles that are retained on the sand collector divided by the number of nanoparticles that strike the sand collector), η_0 is the theoretical single collector efficiency (i.e., number of nanoparticles that strike the sand collector divided by the number of nanoparticles that approach the sand collector) and d_c is the mean diameter of the collector (sand grain). In this analysis η_0 is estimated using the relationship of Nelson and Ginn [39]. Model parameters are presented in Table S5.

Colloid filtration theory suggests that the travel distance of 99% of the nanoparticles formed will be 5.6 m prior to being deposited on the sand grain surface. This is a significant travel distance, and could be especially important where populations have situated groundwater wells in the vicinity of surface waters for bank filtration of pathogens. This analysis implicitly assumes that the nanoparticles are metastable, with limited aggregation and sedimentation. This is a reasonable assumption given the potential for NOM to encapsulate and stabilize nanoparticles[41]. This analysis also makes the simplifying assumption that the nanoparticles are chemically inert and do not dissolve. However, in the case presented here iron oxide nanoparticles will only remain as discrete nanoparticles in the oxic/anaerobic transition zone. As the nanoparticles move deeper to strongly reducing conditions the nanoparticles are likely to dissolve. However, larger oxic/anaerobic transitions zones, either arising due to lower organic matter reactivity or faster flow rates, will enable longer nanoparticle travel distances. Furthermore, when reduced waters rich in dissolved Fe(II), for example in the hyporheic zone, contact oxygenated water, for example at the surface water interface or where oxygenated groundwater is present, colloids may again precipitate and potentially transport As.

382 *Reactive transport mechanism for nanoparticle formation at Elfin Crossing*

383 The exchange of river water with the hyporheic zone and shallow aquifer at Elfin Crossing
384 provides NOM for subsurface microbial communities leading to the titration of electron
385 acceptors which include both dissolved species (DO, NO_3^-) and solids (Mn and Fe
386 oxyhydroxides). A previous sampling campaign in 2009 (data not shown) showed the
387 characteristic loss of dissolved oxygen and corresponding increases in Fe(II) and alkalinity,
388 consistent with the mineralization of NOM by hyporheic microbial communities. Dissolved
389 phosphorus and arsenic also increased in concentration along the flow path as shown here.

390 The results of this study show that colloidal and nanoparticulate Fe oxides are generated
391 within the hyporheic zone. A plausible mechanism for the evolution of Fe nanoparticles
392 within the hyporheic zone is presented in the graphical abstract. We suggest there are two
393 important mechanisms driving the exchange of this hyporheic pore water: (1) Large events
394 which create an enhanced flow gradient from the oxic, and higher DOC surface water to the
395 sub-oxic aquifer, and (2) fluctuations in respiration and photosynthesis in the river water
396 column driving diurnal oscillations in the dissolved oxygen extinction depth. Both
397 mechanisms may cause changes in the depth of O_2 penetration, allowing reduced [Fe(II)-rich]
398 and oxygenated waters to come into contact within the mid-hyporheic zone, thereby allowing
399 the formation of Fe-oxide nanoparticles which have been described here.

400 *Environmental Significance*

401 This study extends our understanding of As interactions with Fe-bearing colloids and
402 nanoparticles in aquifers[19, 22] by demonstrating that As consistently associates with
403 nanoparticle surfaces, but is limited by competition from P. Thus, adsorption of As and P to
404 Fe-bearing nanoparticles essentially mirrors their adsorption behaviour with Fe oxides in the

aquifer matrix[10], but because nanoparticles are mobile and currently unaccounted for in models of As mobility[44], this has important implications for understanding As dynamics in aquifers worldwide. This is because nanoparticles are likely to be particularly important for As mobility where large oxic/anoxic transition zones exist (e.g. between streams and aquifers), or for As transport from anoxic zones into oxic zones, such as at sites of groundwater discharge to surface waters.

ASSOCIATED CONTENT

Supporting Information.. Table S1-S5, Figures S1-S6. This material is available free of charge via the Internet at http://pubs.acs.org.

AUTHOR INFORMATION

Corresponding Author

*Adam Hartland (a.hartland@waikato.ac.nz)

Author Contributions

The manuscript was written through contributions of all authors. All authors have given approval to the final version of the manuscript.

Funding Sources

Funding for this research was provided by the National Centre for Groundwater Research and Training, an Australian Government initiative, supported by the Australian Research Council and the National Water Commission.

ABBREVIATIONS

426 NOM, natural organic matter; DOM, dissolved organic matter; DIC, dissolved inorganic

427 carbon; SW-GW, surface water groundwater.

428 REFERENCES

429 1. Chowdhury, U. K.; Biswas, B. K.; Chowdhury, T. R.; Samanta, G.; Mandal, B. K.;
430 Basu, G. C.; Chanda, C. R.; Lodh, D.; Saha, K. C.; Mukherjee, S. K.; Roy, S.; Kabir, S.;
431 Quamruzzaman, Q.; Chakraborti, D., Groundwater arsenic contamination in Bangladesh and
432 West Bengal, India. *Environmental Health Perspectives* **2000,** *108*, (5), 393-397.
433 2. Rahman, M. M.; Chowdhury, U. K.; Mukherjee, S. C.; Mondal, B. K.; Paul, K.; Lodh,
434 D.; Biswas, B. K.; Chanda, C. R.; Basu, G. K.; Saha, K. C.; Roy, S.; Das, R.; Palit, S. K.;
435 Quamruzzaman, Q.; Chakraborti, D., Chronic arsenic toxicity in Bangladesh and West
436 Bengal, India - A review and commentary. *Journal of Toxicology - Clinical Toxicology* **2001,**
437 *39*, (7), 683-700.
438 3. Chakraborti, D.; Rahman, M. M.; Paul, K.; Chowdhury, U. K.; Sengupta, M. K.;
439 Lodh, D.; Chanda, C. R.; Saha, K. C.; Mukherjee, S. C., Arsenic calamity in the Indian
440 subcontinent: What lessons have been learned? *Talanta* **2002,** *58*, (1), 3-22.
441 4. Bauer, M.; Blodau, C., Mobilization of arsenic by dissolved organic matter from iron
442 oxides, soils and sediments. *Science of the Total Environment* **2006,** *354*, (2-3), 179-190.
443 5. Wang, Y.; Xie, X.; Johnson, T. M.; Lundstrom, C. C.; Ellis, A.; Wang, X.; Duan, M.;
444 Li, J., Coupled iron, sulfur and carbon isotope evidences for arsenic enrichment in
445 groundwater. *Journal of Hydrology* **2014,** *519*, (PA), 414-422.
446 6. Nickson, R.; McArthur, J.; Burgess, W.; Ahmed, K. M.; Ravenscroft, P.; Rahmann,
447 M., Arsenic poisoning of Bangladesh groundwater. *Nature* **1998,** *395*, (6700), 338-338.
448 7. Nickson, R. T.; McArthur, J. M.; Ravenscroft, P.; Burgess, W. G.; Ahmed, K. M.,
449 Mechanism of arsenic release to groundwater, Bangladesh and West Bengal. *Applied*
450 *Geochemistry* **2000,** *15*, (4), 403-413.
451 8. Zheng, Y.; Stute, M.; Van Geen, A.; Gavrieli, I.; Dhar, R.; Simpson, H. J.; Schlosser,
452 P.; Ahmed, K. M., Redox control of arsenic mobilization in Bangladesh groundwater.
453 *Applied Geochemistry* **2004,** *19*, (2), 201-214.
454 9. Horneman, A.; van Geen, A.; Kent, D. V.; Mathe, P. E.; Zheng, Y.; Dhar, R. K.;
455 O'Connell, S.; Hoque, M. A.; Aziz, Z.; Shamsudduha, M.; Seddique, A. A.; Ahmed, K. M.,
456 Decoupling of As and Fe release to Bangladesh groundwater under reducing conditions. Part
457 I: Evidence from sediment profiles. *Geochimica et Cosmochimica Acta* **2004,** *68*, (17), 3459-
458 3473.
459 10. Thi Hoa Mai, N.; Postma, D.; Thi Kim Trang, P.; Jessen, S.; Hung Viet, P.; Larsen,
460 F., Adsorption and desorption of arsenic to aquifer sediment on the Red River floodplain at
461 Nam Du, Vietnam. *Geochimica et Cosmochimica Acta* **2014,** *142*, (0), 587-600.
462 11. Radloff, K. A.; Cheng, Z.; Rahman, M. W.; Ahmed, K. M.; Mailloux, B. J.; Juhl, A.
463 R.; Schlosser, P.; van Geen, A., Mobilization of Arsenic During One-Year Incubations of
464 Grey Aquifer Sands from Araihazar, Bangladesh. *Environmental Science & Technology*
465 **2007,** *41*, (10), 3639-3645.
466 12. Itai, T.; Takahashi, Y.; Seddique, A. A.; Maruoka, T.; Mitamura, M., Variations in the
467 redox state of As and Fe measured by X-ray absorption spectroscopy in aquifers of
468 Bangladesh and their effect on As adsorption. *Applied Geochemistry* **2010,** *25*, (1), 34-47.
469 13. Dzombak, D. A.; Morel, F. M. M., *Surface Complexation Modeling: Hydrous Ferric*
470 *Oxide*. Wiley-Interscience: New York, 1990.

14. van Geen, A.; Bostick, B. C.; Thi Kim Trang, P.; Lan, V. M.; Mai, N.-N.; Manh, P. D.; Viet, P. H.; Radloff, K.; Aziz, Z.; Mey, J. L.; Stahl, M. O.; Harvey, C. F.; Oates, P.; Weinman, B.; Stengel, C.; Frei, F.; Kipfer, R.; Berg, M., Retardation of arsenic transport through a Pleistocene aquifer. *Nature* **2013,** *501*, (7466), 204-207.
15. Burton, E. D.; Johnston, S. G.; Planer-Friedrich, B., Coupling of arsenic mobility to sulfur transformations during microbial sulfate reduction in the presence and absence of humic acid. *Chemical Geology* **2013,** *343*, 12-24.
16. Lapworth, D. J.; Stolpe, B.; Williams, P. J.; Gooddy, D. C.; Lead, J. R., Characterization of suboxic groundwater colloids using a multi-method approach. *Environmental Science and Technology* **2013,** *47*, (6), 2554-2561.
17. Lyvén, B.; Hassellöv, M.; Turner, D. R.; Haraldsson, C.; Andersson, K., Competition between iron- and carbon-based colloidal carriers for trace metals in a freshwater assessed using flow field-flow fractionation coupled to ICPMS. *Geochimica et Cosmochimica Acta* **2003,** *67*, (20), 3791-3802.
18. Hassellöv, M.; von der Kammer, F., Iron oxides as geochemical nanovectors for metal transport in soil-river systems. *Elements* **2008,** *4*, (6), 401-406.
19. Majumder, S.; Nath, B.; Sarkar, S.; Chatterjee, D.; Roman-Ross, G.; Hidalgo, M., Size-fractionation of groundwater arsenic in alluvial aquifers of West Bengal, India: The role of organic and inorganic colloids. *Science of the Total Environment* **2014,** *468-469*, 468-469.
20. Guo, H.; Zhan, B.; Yang, S.; Li, Y.; Stüben, D.; Norra, S.; Wang, J., Role of colloidal particles for hydrogeochemistry in As-affected aquifers of the Hetao Basin, Inner Mongolia. *Geochemical Journal* **2009,** *43*, (4), 227-234.
21. Guo, H.; Zhang, B.; Zhang, Y., Control of organic and iron colloids on arsenic partition and transport in high arsenic groundwaters in the Hetao basin, Inner Mongolia. *Applied Geochemistry* **2011,** *26*, (3), 360-370.
22. Garnier, J. M.; Hurel, C.; Garnier, J.; Lenoble, V.; Garnier, C.; Ahmed, K. M.; Rose, J., Strong chemical evidence for high Fe(II)-colloids and low As-bearing colloids (200nm-10kDa) contents in groundwater and flooded paddy fields in Bangladesh: A size fractionation approach. *Applied Geochemistry* **2011,** *26*, (9-10), 1665-1672.
23. Sharma, P.; Ofner, J.; Kappler, A., Formation of binary and ternary colloids and dissolved complexes of organic matter, Fe and As. *Environmental Science and Technology* **2010,** *44*, (12), 4479-4485.
24. Sharma, P.; Rolle, M.; Kocar, B.; Fendorf, S.; Kappler, A., Influence of natural organic matter on as transport and retention. *Environmental Science and Technology* **2011,** *45*, (2), 546-553.
25. Parks, G. A., The Isoelectric Points of Solid Oxides, Solid Hydroxides, and Aqueous Hydroxo Complex Systems. *Chemical Reviews* **1965,** *65*, (2), 177-198.
26. McArthur, J. M.; Ravenscroft, P.; Safiulla, S.; Thirlwall, M. F., Arsenic in groundwater: Testing pollution mechanisms for sedimentary aquifers in Bangladesh. *Water Resources Research* **2001,** *37*, (1), 109-117.
27. McArthur, J. M.; Banerjee, D. M.; Hudson-Edwards, K. A.; Mishra, R.; Purohit, R.; Ravenscroft, P.; Cronin, A.; Howarth, R. J.; Chatterjee, A.; Talukder, T.; Lowry, D.; Houghton, S.; Chadha, D. K., Natural organic matter in sedimentary basins and its relation to arsenic in anoxic ground water: The example of West Bengal and its worldwide implications. *Applied Geochemistry* **2004,** *19*, (8), 1255-1293.
28. Neumann, R. B.; Ashfaque, K. N.; Badruzzaman, A. B. M.; Ashraf Ali, M.; Shoemaker, J. K.; Harvey, C. F., Anthropogenic influences on groundwater arsenic concentrations in Bangladesh. *Nature Geosci* **2010,** *3*, (1), 46-52.

29. Neumann, R. B.; Pracht, L. E.; Polizzotto, M. L.; Badruzzaman, A. B. M.; Ali, M. A., Sealing rice field boundaries in Bangladesh: A pilot study demonstrating reductions in water use, arsenic loading to field soils, and methane emissions from irrigation water. *Environmental Science and Technology* **2014,** *48*, (16), 9632-9640.
30. Harvey, C. F.; Ashfaque, K. N.; Yu, W.; Badruzzaman, A. B. M.; Ali, M. A.; Oates, P. M.; Michael, H. A.; Neumann, R. B.; Beckie, R.; Islam, S.; Ahmed, M. F., Groundwater dynamics and arsenic contamination in Bangladesh. *Chemical Geology* **2006,** *228*, (1–3), 112-136.
31. Biksey, T. M.; Gross, E. D., The hyporheic zone: Linking groundwater and surface water—understanding the paradigm. *Remediation Journal* **2001,** *12*, (1), 55-62.
32. Nimick, D. A.; Gammons, C. H.; Parker, S. R., Diel biogeochemical processes and their effect on the aqueous chemistry of streams: A review. *Chemical Geology* **2011,** *283*, (1–2), 3-17.
33. Andersen, M. S.; Acworth, R. I., Stream-aquifer interactions in the Maules Creek catchment, Namoi Valley, New South Wales, Australia. *Hydrogeology Journal* **2009,** *17*, (8), 2005-2021.
34. Baalousha, M.; Lead, J. R., Characterization of natural and manufactured nanoparticles by atomic force microscopy: Effect of analysis mode, environment and sample preparation. *Colloids and Surfaces A: Physicochemical and Engineering Aspects* **2013,** *419*, 238-247.
35. Baalousha, M.; Lead, J. R., Rationalizing nanomaterial sizes measured by atomic force microscopy, flow field-flow fractionation, and dynamic light scattering: Sample preparation, polydispersity, and particle structure. *Environmental Science and Technology* **2012,** *46*, (11), 6134-6142.
36. Baalousha, M.; Prasad, A.; Lead, J. R., Quantitative measurement of the nanoparticle size and number concentration from liquid suspensions by atomic force microscopy. *Environmental Sciences: Processes and Impacts* **2014,** *16*, (6), 1338-1347.
37. Hartland, A.; Baker, A.; Timms, W.; Shutova, Y.; Yu, D., Measuring dissolved organic carbon δ13C in freshwaters using total organic carbon cavity ring-down spectroscopy (TOC-CRDS). *Environ Chem Lett* **2012,** *10*, (3), 309-315.
38. Tufenkji, N.; Elimelech, M., Correlation Equation for Predicting Single-Collector Efficiency in Physicochemical Filtration in Saturated Porous Media. *Environmental Science & Technology* **2004,** *38*, (2), 529-536.
39. Nelson, K. E.; Ginn, T. R., New collector efficiency equation for colloid filtration in both natural and engineered flow conditions. *Water Resources Research* **2011,** *47*.
40. Ma, H.; Johnson, W. P., Colloid Retention in Porous Media of Various Porosities: Predictions by the Hemispheres-in-Cell Model. *Langmuir* **2010,** *26*, (3), 1680-1687.
41. Buffle, J.; Leppard, G. G., Characterization of Aquatic Colloids and Macromolecules. 1. Structure and Behavior of Colloidal Material. *Environmental Science & Technology* **1995,** *29*, (9), 2169-2175.
42. Lead, J. R.; Wilkinson, K. J., Aquatic Colloids and Nanoparticles: Current Knowledge and Future Trends. *Environmental Chemistry* **2006,** *3*, (3), 159-171.
43. Yao, K. M.; Habibian, M. M.; O'Melia, C. R., Water and waste water filtration – Concepts and applications. *Environ. Sci. Technol.* **1971,** *5*, 1105–1971.
44. Radloff, K. A.; Zheng, Y.; Michael, H. A.; Stute, M.; Bostick, B. C.; Mihajlov, I.; Bounds, M.; Huq, M. R.; Choudhury, I.; Rahman, M. W.; Schlosser, P.; Ahmed, K. M.; van Geen, A., Arsenic migration to deep groundwater in Bangladesh influenced by adsorption and water demand. *Nature Geosci* **2011,** *4*, (11), 793-798.

568

569 **Table 1.** Average particle size derived from atomic force microscopy (AFM) imaging of
570 Maules Creek samples.

Sample	Average size of all particles (raw data)	Average size of all particles ≤25 nm (raw data)	Fitted Log normal distribution model	% fraction > 25 nm
River	10.2±17.9	4.6±5.1	2.3±0.8	1.7
Hyporheic (0.5m)	1.7±1.0	1.7±1.0	1.9±0.6	0
Hyporheic (1.0m)	6.5±6.5	6.0±5.5	5.0±2.9	1.9
Hyporheic (1.5m)	9.0±3.2	9.0±3.2	9.8±3.0	0
Shallow GW (E4)	5.8±3.4	5.8±3.4	6.2±3.9	0
Regional GW (MBH)	9.3±12.0	4.8±6.4	2.2±0.8	19.3

571

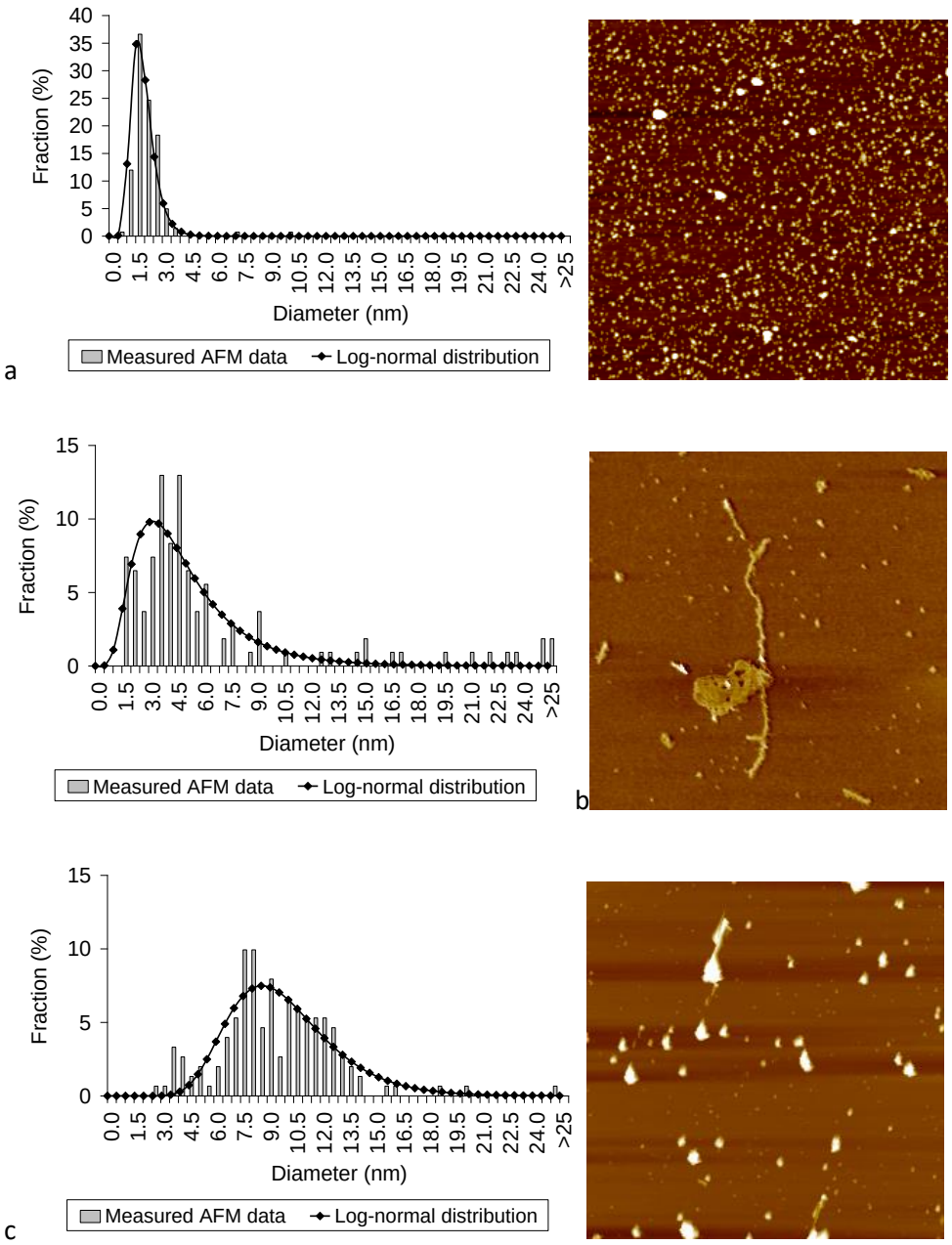

572

573 **Figure 1**. Results of atomic force microscopy (AFM) imaging and calculated number particle
574 distributions with Log-normal distribution fit for hyporheic piezometers (a = 0.5 m; b= 1.0 m
575 and c = 1.5 m). AFM micrographs displayed at 3 x 3 μm magnification.

576

577

578

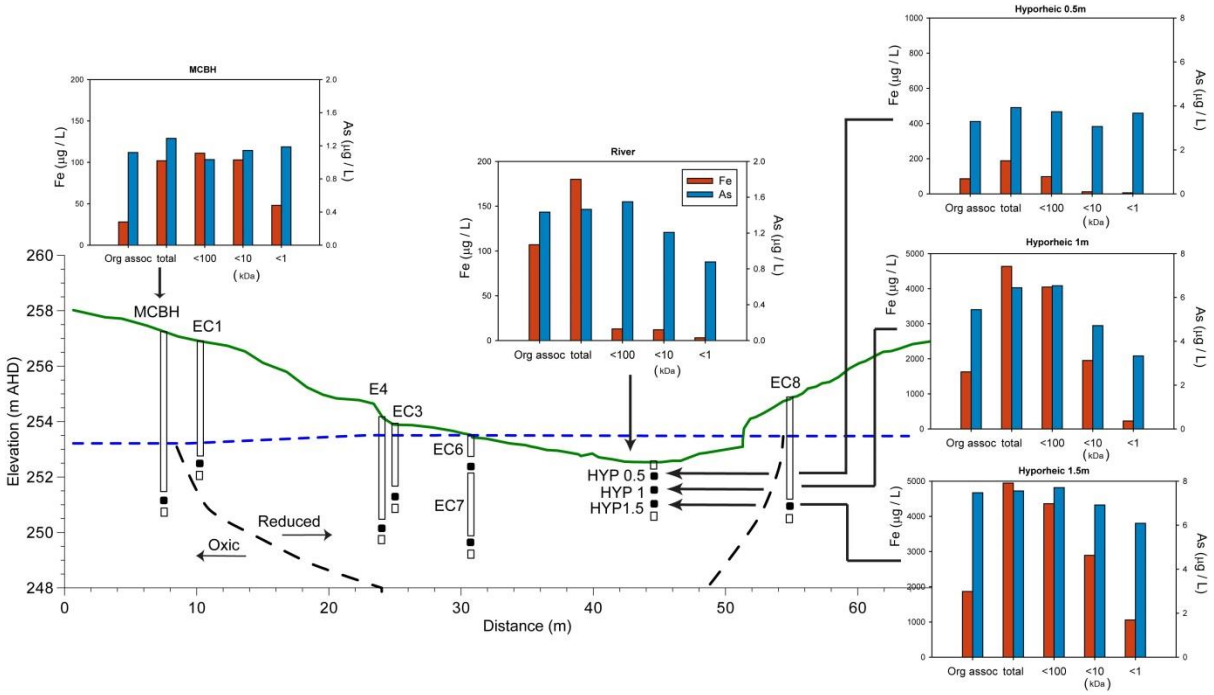

Figure 2. Cross-sectional representation of the study site at Maules Creek, showing the piezometric surface relative to the river water level (blue dashed line) and locations and screen depths of the piezometers. Representative data from ultrafiltered fractions is shown for (a) regional groundwater, (b) river water, and (c) the hyporheic zone at depths of 0.5, 1.0 and 1.5 m. Iron (Fe) and arsenic (As) concentrations shown by red bars and blue bars, respectively. Org assoc = concentration of trace element retained by ENV+ resin.

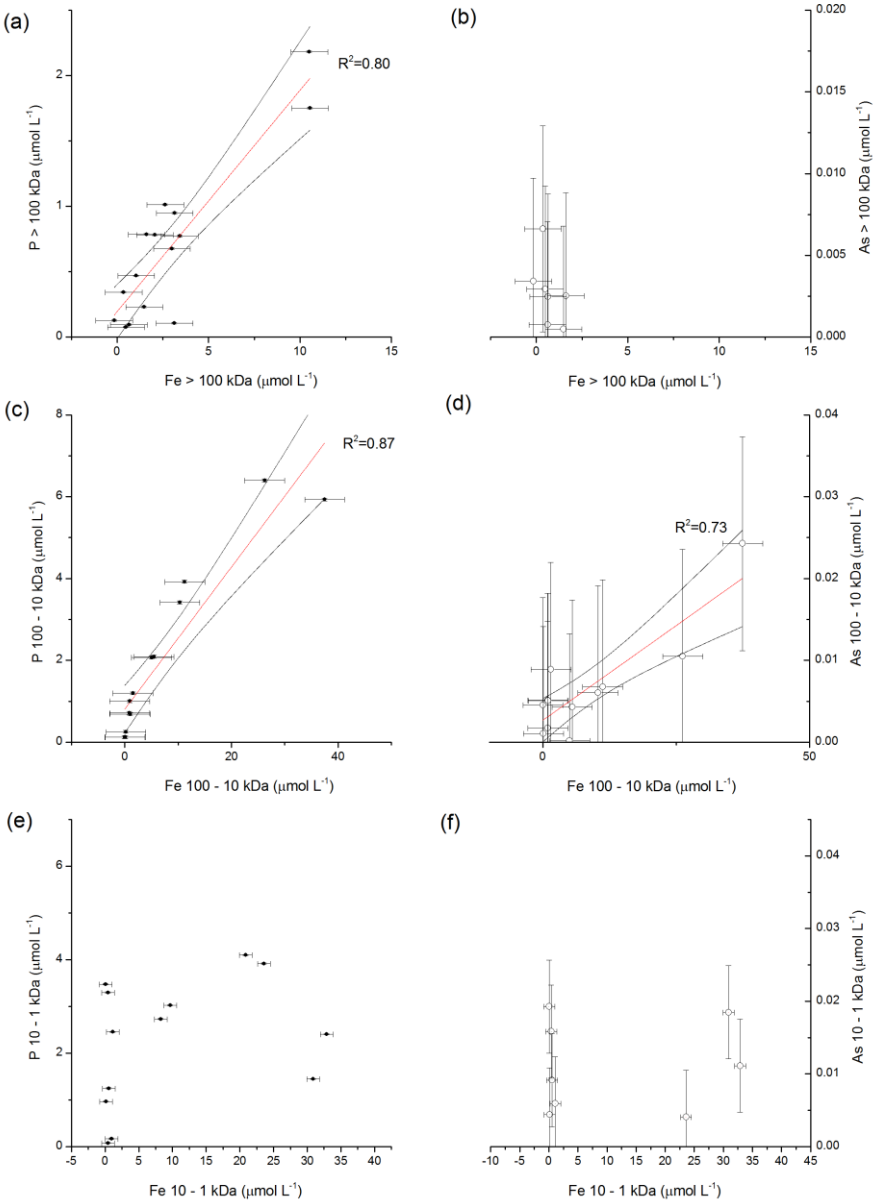

586

587 **Figure 3.** Distribution of As (o) and P (♦) in fractionated water samples from Maules Creek
588 as a function of the Fe concentration in the same fraction. (a-b) > 100 kDa, (c-d) 100 – 10
589 kDa, (e-f) 10 – 1 kDa. Red lines are least squares fits and dark lines are 95% confidence
590 bands (a, c and d). Error bars are the cumulative pooled standard deviations determined from
591 four replicated procedural analyses.

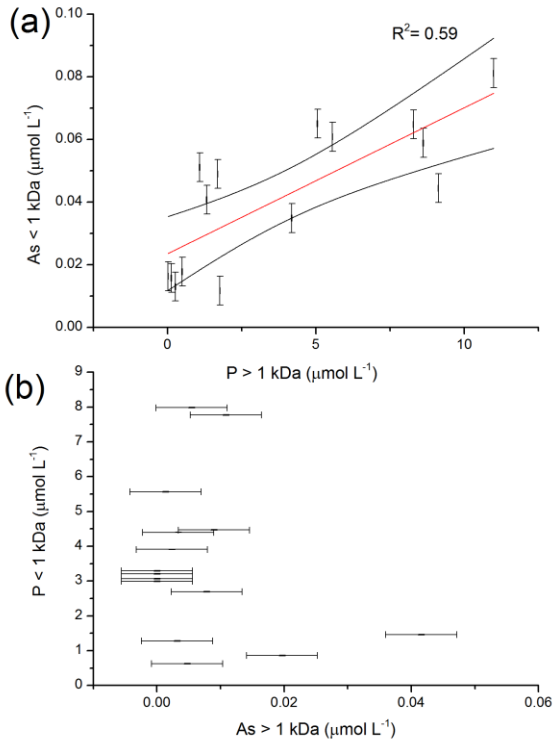

592

593 **Figure 4**. Evidence for competitive adsorption between P and As in the presence of iron-
594 bearing nanoparticles in Maules Creek surface water and groundwaters. Data presented are
595 solution concentrations in ultrafiltered fractions.

596